

## Tuning the directionality of spin waves generated by femtosecond laser pulses in a garnet film by optically driven ferromagnetic resonance

A. E. Khramova,<sup>1,2</sup> M. Kobecki,<sup>3</sup> I. A. Akimov<sup>1b,3,6</sup>, I. V. Savochkin<sup>1b,1,2</sup>, M. A. Kozhaev,<sup>1,4</sup> A. N. Shaposhnikov<sup>1b,5</sup>, V. N. Berzhansky,<sup>5</sup> A. K. Zvezdin,<sup>1,4,7</sup> M. Bayer,<sup>3,6</sup> and V. I. Belotelov<sup>1b,1,2,5</sup>

<sup>1</sup>*Russian Quantum Center, 45, Skolkovskoye shosse, Moscow 121353, Russia*

<sup>2</sup>*Faculty of Physics, Lomonosov Moscow State University, Leninskie Gory, Moscow 119991, Russia*


<sup>3</sup>*TU Dortmund, Experimentelle Physik 2, D-44221 Dortmund, Germany*

<sup>4</sup>*Prokhorov General Physics Institute RAS, 38 Vavilov Street, Moscow 119991, Russia*

<sup>5</sup>*Vernadsky Crimean Federal University, 4 Vernadskogo Prospekt, Simferopol 295007, Crimea*

<sup>6</sup>*Ioffe Institute, Russian Academy of Sciences, 194021 St. Petersburg, Russia*

<sup>7</sup>*NTI Center for Quantum Communications, National University of Science and Technology MISiS, Leninsky Prospekt 4, Moscow 119049, Russia*

 (Received 30 May 2022; revised 3 October 2022; accepted 1 November 2022; published 13 February 2023)

Excitation of spin waves of a required frequency and directional spectrum is among the crucial tasks in optomagnonics. Here we investigate the generation of spin waves in an iron garnet thin film by a train of femtosecond laser pulses with ultimately high repetition rate of up to 10 GHz and compare it with the case of 1-GHz repetition rate. The periodic optical excitation with repetition rate close to the frequency of the ferromagnetic resonance amplifies spin waves with particular phase velocity and wavelength, which are tunable across a wide range by small variations of the frequency detuning, and can be adjusted by the magnitude of the applied external magnetic field. For pulses of the same fluence, the 10-GHz pulse rate provides a significant resonant increase of the spin-wave amplitude by 11.5 times with respect to single-pulse excitation while the 1-GHz pulse rate provides only a 1.5 times advancement. Moreover, variation of the detuning frequency provides different regimes of the spin-wave propagation: short- and long-distance propagation along the magnetic field direction and appearance of an “X” line shape in the directionality pattern, making the considered optical approach of spin-wave generation promising for designing magnonic devices.

DOI: [10.1103/PhysRevB.107.064415](https://doi.org/10.1103/PhysRevB.107.064415)

### I. INTRODUCTION

Ultrafast magnetization dynamics in ferromagnetic materials under excitation with femtosecond (fs) laser pulses was first demonstrated in Ni thin films at the end of the previous century, when the phenomenon of ultrafast demagnetization was revealed [1]. Although the impact of light had a thermal character in this case, it exhibits a fast magnetic response on timescales of subpicoseconds and, moreover, it provided the basis of ultrafast all-optical magnetic switching, demonstrated shortly after [2–5]. On the other hand, a nonthermal optical impact on spins was demonstrated almost two decades ago in a magnetic dielectric crystal of DyFeO<sub>3</sub> [6] and a magnetic thin film of iron garnet [7], where circularly polarized femtosecond laser pulses were used to induce a precession of the magnetization. Later, excitation of magnetostatic spin waves by fs laser pulses was also demonstrated in Refs. [8–15], taking place due to optomagnetic effects, in particular the inverse magneto-optical Faraday effect, which can be considered as an effective magnetic field induced by circularly polarized light while it propagates through a magnetic medium [16–18]. The effective magnetic field exists in a magnetic film only in presence of the optical field, the time dependence of which is limited by the laser-pulse duration of about 100 fs. This

timescale is three orders of magnitude shorter than the period of magnetization precession, and, therefore, the impact can be considered as instantaneous.

Coherent control of magnetization precession was further performed by excitation with two pump-laser pulses, which were delayed with respect to each other by a half or a full precession period of magnetization. This allowed one to obtain either destructive or constructive interference for the excitation of spin precession in magnetic media [7].

Optical methods for excitation of spin waves by laser pulses are appealing as compared to conventional microwave techniques since they provide a local impact on the magnetization within a spot size limited only by the Rayleigh criterion. The laser spot can be easily controlled and varied: one can move it all over the sample, change its size, and modify the optically induced effective magnetic field by adjusting the pump polarization. At the same time, laser pulses excite a rather broad spectrum of spin waves in case of tight focusing.

The next step toward all-optical generation of spin waves in magnetic media was taken in Refs. [10,19–21] where an approach based on excitation with multiple pulses was implemented. Thereby, a sample was illuminated by a comb of pump pulses, which trigger the magnetization at a repetition rate of 1 GHz, comparable with the magnetization precession

frequency, i.e., the frequency of magnetic resonance. At such a high repetition rate, the subsequent pump pulse arrives before decay of the magnetization precession that was launched by the previous pulse, so that an accumulation effect takes place. Spin-wave emission is sustained continuously then. As a result, the periodic pumping allows one to keep locality of the impact and, at the same time, makes the spin-wave spectrum narrower. The multiple pump-pulse regime provides spin-wave directionality with respect to the magnetic field orientation [10].

Recently, such periodic pumping at 1-GHz rate was also applied to a permalloy thin film, where selective spin-wave mode excitation [22] and X-shaped caustic spin-wave patterns [23] were demonstrated. Due to the metallic character of the permalloy system, optical generation of spin waves was achieved via ultrafast demagnetization and consequent thermal energy transfer to magnons in the ferromagnetic layer [24]. This is in contrast to magnetic dielectrics such as iron garnet films where the inverse Faraday effect has a direct impact on the magnetization as mentioned above. In those experiments (Refs. [10,19]), the repetition rate of the pumping pulses allowed us to excite relatively large numbered precession harmonics. At the same time, the excitation efficiency for lower-numbered harmonics should be higher. Moreover, the first-order harmonic, corresponding to the ferromagnetic resonance, was not attained. Optical excitation of the ferromagnetic resonance is quite crucial for extending the capabilities of ultrafast optical triggers for magnonics.

In this work, we investigate the impact of multiple-pulse excitation further and consider optical pumping of an iron garnet film with a train of femtosecond laser pulses with a very high repetition rate of 10 GHz. At such high repetition rate, it is possible to have only one precession cycle in between two consecutive laser pulses, which corresponds to the regime of optically driven ferromagnetic resonance. The amplitude of the excited spin waves is resonantly increased when their frequency is tuned to the pulse repetition rate by an external magnetic field, corresponding to the resonance condition between the repetition rate  $f_{\text{rep}}$  and the frequency of ferromagnetic resonance  $\nu$ . By variation of the external magnetic field we change the detuning frequency  $\Delta = (\nu - f_{\text{rep}})/f_{\text{rep}}$  and compare the spin-wave directionality diagram for three cases in which the external magnetic field strength is below the resonant one (negative detuning  $\Delta < 0$ ), equal to it (resonant case), and exceeds that field ( $\Delta > 0$ ). We find that the spin-wave propagation and directionality pattern are quite different in these three cases showing either short- or long-distance propagation mainly along the external field direction or an X-shape directionality pattern.

## II. MATERIALS AND METHODS

The experimental studies were performed on a transparent monocrystalline ferrimagnetic film of bismuth-substituted iron garnet  $(\text{Bi}_{0.9}\text{Lu}_{1.4}\text{Tm}_{0.4}\text{Y}_{0.2}\text{Sm}_{0.1})(\text{Fe}_{4.4}\text{Ga}_{0.6})\text{O}_{12}$ . The film was grown on a gadolinium gallium garnet substrate with crystallographic orientation [111] by liquid-phase epitaxy. The film thickness is 5  $\mu\text{m}$ , the saturation magnetization is  $4\pi M_s = 480$  G, the uniaxial anisotropy constant is  $K_u = 5 \times 10^3 \frac{\text{erg}}{\text{cm}^3}$ , the cubic anisotropy constant is  $K_1 = 2 \times 10^3 \frac{\text{erg}}{\text{cm}^3}$ ,

and the Gilbert constant is  $\alpha = 0.01$ . The saturation magnetization and the cubic anisotropy constant were estimated from the film composition [25], while the uniaxial anisotropy constant and the Gilbert damping were found from the ferromagnetic resonance spectra. The sample was placed in a quasiuniform external magnetic field  $H$  created by an electromagnet. The direction of the magnetic field was in the sample plane [Fig. 1(a)]. All measurements were performed at room temperature.

We study the excitation and detection of spin waves using time-resolved pump-probe Faraday rotation with asynchronous optical sampling. In this case two synchronized Ti:sapphire oscillators are used as sources of the pump and probe pulses with a duration of  $\Delta t = 50$  fs. The probe beam with 1-GHz repetition rate is supplied by the master oscillator (Gigajet TWIN 20c/20c from LaserQuantum), while the pump beam is emitted by one of two slave oscillators with either 1- or 10-GHz (Taccor  $\times 10$  from LaserQuantum) repetition rate. Each of the slave oscillators is synchronized to the master oscillator with an offset frequency of 2 kHz, which allows us to acquire the pump-probe transients using a fast photodiode in combination with a digitizer card giving an overall time resolution around 1 ps. The pump wavelength is set to 810 nm. The center wavelength of the probe is set to a value around 760 nm, which allows us to filter spectrally the stray light by a bandpass interference filter placed in the detection path.

Both beams are focused on the sample using a reflective microscope with  $15\times$  magnification to a spot size of approximately 8  $\mu\text{m}$  in diameter (full width at half maximum). The incidence angle for both the pump and probe beams was about  $17^\circ$  relative to the normal, with incidence planes oriented orthogonal to each other. The pump beam is directed into the objective via a piezomirror, which enables scanning the distance between the pump and probe spots in the  $xy$  plane. Before focusing on the sample, the pump beam passes through a Glan prism and a quarter-wave plate to obtain circularly polarized pulses. Circular polarization of the pump pulses is required for an effective action on spins through the inverse Faraday effect (IFE) [26]. In this case, the impact of the illumination can be described in terms of pulses of an effective magnetic field  $\mathbf{H}_{\text{IFE}}$  induced via the inverse Faraday effect and directed along the wave vector of the excitation beam, which is close to normal. In our sample with a thickness of only a few micrometers, the effective field is homogeneous along the direction perpendicular to the sample plane and its time duration is the same as that of the optical pulse.

Observation of the excited spin dynamics is accomplished via the Faraday effect of the probe pulses in transmission geometry. Before focusing on the sample, the probe pulses are linearly polarized by passing through a Glan prism. The probe pulses transmitted through the sample are then collected and collimated by an identical objective. As the Faraday effect is determined by the component of the magnetization parallel to the light wave vector, the probe pulses are sensitive to the out-of-plane  $z$  component of the precessing magnetization [see Fig. 1(a)]. The oscillating out-of-plane magnetic component is directly proportional to the Faraday rotation angle  $\psi$  of the transmitted probe pulses. The angle of rotation is measured using a differential scheme based on a Wollaston prism and a balanced photodiode. The differential signal from

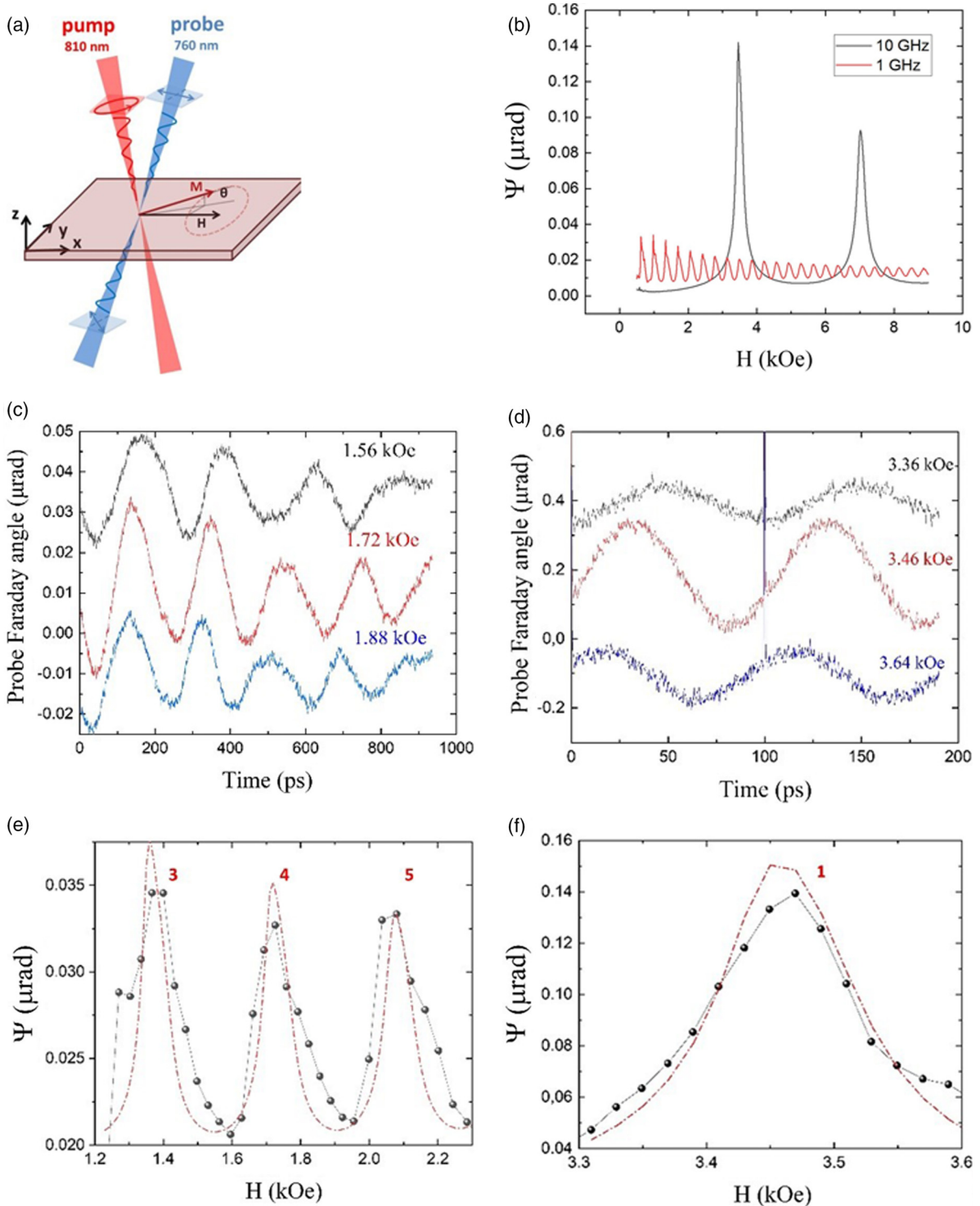


FIG. 1. (a) Scheme of the experiment. (b) Calculated dependence of the magnetization precession amplitude  $\theta_0$  on the magnetic field for two repetition rates of the laser pump pulses: 1 and 10 GHz. When the precession frequency is a multiple of the pump repetition rate, numerous resonant peaks appear. All experimental data are normalized for the pump fluence  $15 \mu\text{J}/\text{cm}^2$ . (c) Magnetization precession measured for the pump repetition rate of 1 GHz in the range of magnetic fields of 1.56–1.89 kOe, which corresponds to the fourth resonant peak in (b) (red curve). An increase of the precession amplitude is seen for the magnetic field of 1.72 kOe. (d) Magnetization precession for the pump repetition rate of 10 GHz in the range of magnetic fields of 3.3–3.6 kOe, which corresponds to the first resonant peak (black curve) in (b). A noticeable increase of the precession amplitude is seen for the magnetic field of 3.46 kOe. (e), (f) Dependence of the precession amplitude on the magnetic field for the pulse repetition rates of 1 GHz (e) and 10 GHz (f), respectively. Dotted red lines show the amplitude calculated from the model given by Eq. (1a) and the black lines represent the experimental amplitudes.

the photodetector, amplified by a factor of 1000, was fed into a high-speed digitizer card, triggered by the synchronization unit (TL-1000 LaserQuantum).

### III. RESULTS

Since the effective magnetic field of the inverse Faraday effect  $\mathbf{H}_{\text{IFE}}$  is directed close to the film normal and the magnetization in the ground state is oriented in the film plane, the spins are subject to a torque generated by the pump pulses. The torque initiates their precession around the total magnetic field [Figs. 1(c) and 1(d)]. As shown in our previous works [10,23,27,28], if the frequency of the spin dynamics is a multiple of the pump-pulse repetition rate, a cumulative effect occurs, leading to a resonant increase of the precession amplitude. This condition can be met by changing the in-plane external magnetic field  $H$  since the precession frequency depends on  $H$  as  $\nu = \frac{\gamma}{2\pi} \sqrt{H(H + H_a)}$ , where  $H_a = 4\pi M_s - 2K_u/M_s$ , and  $\gamma$  is the gyromagnetic ratio. Here, we neglect the cubic anisotropy since  $K_1$  is three times smaller than  $K_u$ . Note that  $\nu$  corresponds to the frequency of ferromagnetic resonance. Indeed, the behavior of the spins is described by the Landau-Lifshitz equation, and the initial conditions take into account the instant impact of  $H_{\text{IFE}}(t) = h\Delta t \sum_{m=0}^{+\infty} \delta(t - mT)$ , where  $\delta(t)$  is the Dirac delta function,  $h$  is the amplitude of  $H_{\text{IFE}}$ , and  $\Delta t$  is the pulse duration. As a result, in between two successive laser pulses the magnetization precession is given by a decaying harmonic function:  $\theta(t) = \theta_0 e^{-(t/\tau)} \sin(2\pi\nu t + \zeta)$ , where  $\tau$  is the decay time,  $\theta_0$  and  $\zeta$  are the initial amplitude and phase of the precession, respectively, given by

$$\theta_0 = \frac{\gamma^2 H h \Delta t}{2\pi\nu} (1 - 2e^{-T/\tau} \cos 2\pi\nu T + e^{-2T/\tau})^{-1/2}, \quad (1a)$$

$$\zeta = \text{atan}\{e^{-(T/\tau)} \sin 2\pi\nu T [1 - e^{-T/\tau} \cos 2\pi\nu T]\}, \quad (1b)$$

It follows from Eq. (1a) that if  $\nu T = n$ , where  $n$  is an integer, then the amplitude is maximized. The matching values of the precession frequency can be obtained by adjusting the external magnetic field strength. At resonance, the initial phase  $\zeta = 0$  [see Eq. (1b)]. If the external magnetic field leads to a precession frequency right in the middle between two resonant values, so that  $\nu T = n - 1/2$ , then the antiresonance case takes place where the precession amplitude is minimized to  $\theta_{\text{min}}$ . The factor  $K$  of the amplitude enhancement with respect to single-pulse excitation  $\theta_{\text{SP}}$  is found as

$$K = \frac{\theta_{\text{max}}}{\theta_{\text{SP}}} = (1 - 2e^{-(T/\tau)} + e^{-(2T/\tau)})^{-1/2}. \quad (2)$$

Experimental studies confirm such a behavior of the precession amplitude when varying the external magnetic field. The excited magnetization precession is traced by the probing Faraday angle  $\psi(t) \sim \theta(t)$ , so that the measured signal is  $\psi(t) = \Psi e^{-(t/\tau)} \sin(2\pi\nu t + \zeta)$ . The experimental data were thus approximated by this expression for  $\psi(t)$ , from which the signal amplitude  $\Psi$  was found [Figs. 1(e) and 1(f)].

For the repetition rate of the laser pulses of  $f_{\text{rep}} = 1$  GHz ( $T = 1$  ns) the maximum amplitude  $\Psi_{\text{max}}$  is achieved at  $H = 1.72$  kOe [Figs. 1(c) and 1(e)]. The resonance corresponds to  $n = 5$ . On the other hand, for  $f_{\text{rep}} = 10$  GHz ( $T = 0.1$  ns) the amplitude resonance is of first order ( $n = 1$ ) and appears

at  $H = 3.46$  kOe [Figs. 1(d) and 1(f)]. The figures below show the normalized results. Initially, the energy density of the pump pulse was  $15 \mu\text{J}/\text{cm}^2$  for the excitation frequency of 10 GHz and  $160 \mu\text{J}/\text{cm}^2$  for the excitation frequency of 1 GHz.

Usually, for iron garnets  $\tau > T$  and it is not possible to directly measure  $\tau$ . Nevertheless, the decay time can be found from the ratio of the maximal and minimal amplitudes of precession,  $\kappa = \theta_{\text{max}}/\theta_{\text{min}}$ :

$$\tau = T \ln^{-1} \frac{\kappa + \xi}{\kappa - \xi}, \quad (3)$$

where  $\xi = 1 - 1/2n$ . As follows from Fig. 1(e), for  $T = 1$  ns and  $n = 5$ :  $\kappa = 2.3$ , which, in accordance with Eq. (3), gives  $\tau = 1.1$  ns. Therefore, Eq. (2) provides the enhancement coefficient  $K = 1.7$  for  $T = 1$  ns. If the repetition rate of the pulses is ten times higher,  $T = 0.1$  ns, the enhancement factor is much larger and reaches  $K = 11.5$ .

To trace multiple resonances across a wide range of external magnetic fields we performed micromagnetic modeling using the MUMAX3 platform [21] [Fig. 1(b)]. It is seen that when the magnetic field is swept, the resonances for  $T = 1$  ns excitation appear ten times more frequently than for  $T = 0.1$  ns, while their amplitude is seven times smaller. Here, we assumed that in both cases the pulses carry the same energy, have the same duration, and are focused in spots of equal diameter, so that they therefore produce equal  $H_{\text{IFE}}$ . The latter corresponds well with the data from experiment.

As one could see above, excitation of the spin dynamics with a laser pulse train of higher repetition rate is more efficient if pulses of the same fluence are used. This fact might turn out to be crucial in case of some constrictions on the maximum applicable laser power, e.g., due to sample overheating.

Also, it should be more advantageous for spectral selectivity of the spin waves and therefore provide lower dephasing. Consequently, in what follows we concentrate on the excitation of spin waves with the ultimately high repetition rate of  $f_{\text{rep}} = 10$  GHz ( $T = 0.1$  ns).

The observed spin dynamics is the result of excitation and propagation of magnetostatic spin waves (MSWs). Since the external magnetic field is applied in the film plane (along the  $x$  axis) [Fig. 1(a)], backward-volume MSWs and surface MSWs are expected to contribute. The amplitude of magnetization precession is strongly anisotropic as seen from Fig. 2 where signal strengths measured as function of the distance between the pump and probe beams are summarized for the resonant case with  $\Delta = 0$  [panel (b)], as well as for negative  $\Delta < 0$  (a) and positive  $\Delta > 0$  (c) detuning. The decays of the signal along the  $x$ - and  $y$  axes are shown in the corresponding panels (d)–(f) at the bottom. In the resonant case, the scan along the  $X$  axis (along the magnetic field) shows signal up to  $20 \mu\text{m}$ , while for the scan in the orthogonal direction no signal is detected for distances larger than  $5 \mu\text{m}$  [Figs. 2(b) and 2(e), red and black curves]. This observation indicates that in our case the backward-volume MSWs which propagate mostly along the magnetic field are predominantly excited by the pump. The absence of surface MSWs is due to the relatively large pump beam diameter [8].

Periodic pumping can also lead to peculiar spatial distributions of the MSW amplitude, which is sensitive to the

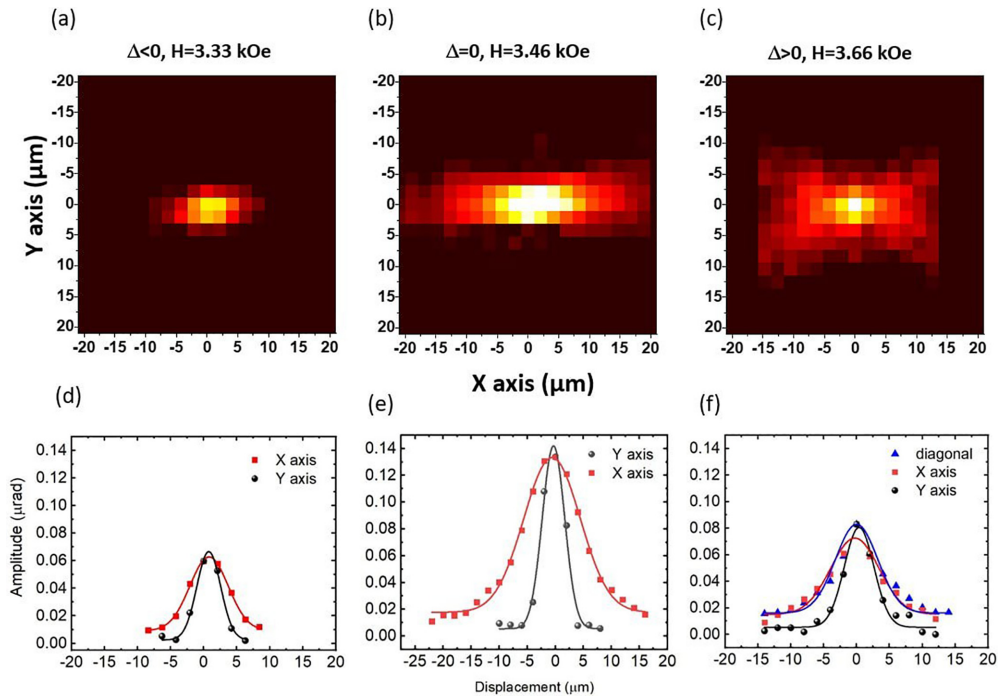


FIG. 2. (a)–(c) Color maps of the measured spatial distribution of the amplitude of the out-of-plane magnetization component of MSWs, accessed through the amplitude of the Faraday rotation angle  $\Psi$  of the probe for three different values of the external magnetic field: (a) below the resonance,  $\Delta < 0 - H = 3.33$  kOe, (b) at the resonance,  $\Delta = 0 - H = 3.46$  kOe, and (c) above the resonance,  $\Delta > 0 - H = 3.66$  kOe. (d)–(f) Dependence of the amplitude of the spin waves on the coordinate along ( $X$  axis, red symbols) and perpendicular ( $Y$  axis, black symbols) to the external magnetic field for  $H = 3.33$  kOe (d),  $H = 3.46$  kOe (e), and  $H = 3.66$  kOe (f). Corresponding solid curves show fits to the experimental data by Gaussian functions (see the text). Laser pulse repetition rate is 10 GHz.

detuning and consequently to the magnetic field. For this reason, we recorded the precession signals not only along the coordinate axes but also at other points around the pumped area (Fig. 2). If the external magnetic field is below resonance, i.e.,  $\Delta < 0$  ( $H = 3.33$  kOe), then the amplitude is rather small and, moreover, the MSWs marginally propagate away from the pumped area [Fig. 2(a)]. Even along the  $X$  axis the signal can hardly be traced beyond the pump spot on the sample.

However, if the external field is set to the resonance, i.e.,  $\Delta = 0$  ( $H = 3.46$  kOe), then the distribution is modified drastically [Fig. 2(b)]. Indeed, the precession amplitude gets three times larger and, most importantly, the oscillations can be traced well along the  $X$  axis for much longer distances, meaning that the propagation distance of the excited MSW wave packet is enhanced. Such an increase of the MSW propagation distance is explained by the narrowing of the MSW spectrum, which diminishes the dephasing rate due to the interference of the different spectral components of excited MSWs. Since the main reason for the MSW wave-packet decay is dephasing, the dependence of its amplitude on a spatial coordinate should be well described by a Gaussian function:  $\theta(r) = \theta_0 e^{-r^2/2\sigma_{\text{MSW}}^2}$ , where  $\sigma_{\text{MSW}}$  is the Gaussian standard deviation, which in our case determines the propagation distance of the MSW wave packet  $L = 2\sigma_{\text{MSW}}$ .

However, the experimentally observed spatial dependence of the MSW wave-packet amplitude  $\Psi(r)$  is a convolution of  $\theta(r)$  with the Gaussian profile of the probe beam:

$$\Psi(r) = \Psi_m e^{-r^2/2\sigma^2}, \quad (4)$$

where  $\sigma^2 = \sigma_{\text{pr}}^2 + \sigma_{\text{MSW}}^2$ , and  $\sigma_{\text{pr}} = 3 \mu\text{m}$  is the Gaussian parameter for the probe beam. Thus, approximating the experimentally measured dependence of the MSW wave-packet amplitude with Eq. (4) [see the solid curves in Figs. 2(d)–2(f)] allows us to quantify the notable increase of the propagation distance along the  $X$  axis. It gives the MSW wave-packet propagation length  $L$  for optical excitation of the ferromagnetic resonance, i.e.,  $L = 12 \mu\text{m}$  for  $\Delta = 0$ , while for  $\Delta < 0$  ( $H = 3.33$  kOe) and  $\Delta > 0$  ( $H = 3.66$  kOe) one gets  $L = 4 \mu\text{m}$  and  $L = 10 \mu\text{m}$ , respectively. Therefore, the MSW wave packet propagates much farther along the magnetic field when matching the resonance condition and moderately long for not too large positive  $\Delta$ . The propagation along the  $Y$  axis remains unchanged at the previous level so that a kind of unidirectional MSW emission is achieved.

An additional degree of freedom appears for magnetic fields exceeding the resonant one. While at  $H = 3.66$  kOe the amplitude diminishes, the propagation diagram modifies its shape to an X-like shape [Fig. 2(c)] and pronounced diagonal components appear.

Actually, a kind of MSW caustics establishes similarly to the caustics observed earlier on a permalloy thin film [28]. However, in the current case the scales of the caustics are larger as compared with propagation length in Ref. [17].

The special feature of our experimental approach is the applied spatially- and time-resolved pump-probe technique, which allows us to monitor the evolution of the magnetization precession phase and consequently to measure directly the phase velocity of the spin wave for a given direction.

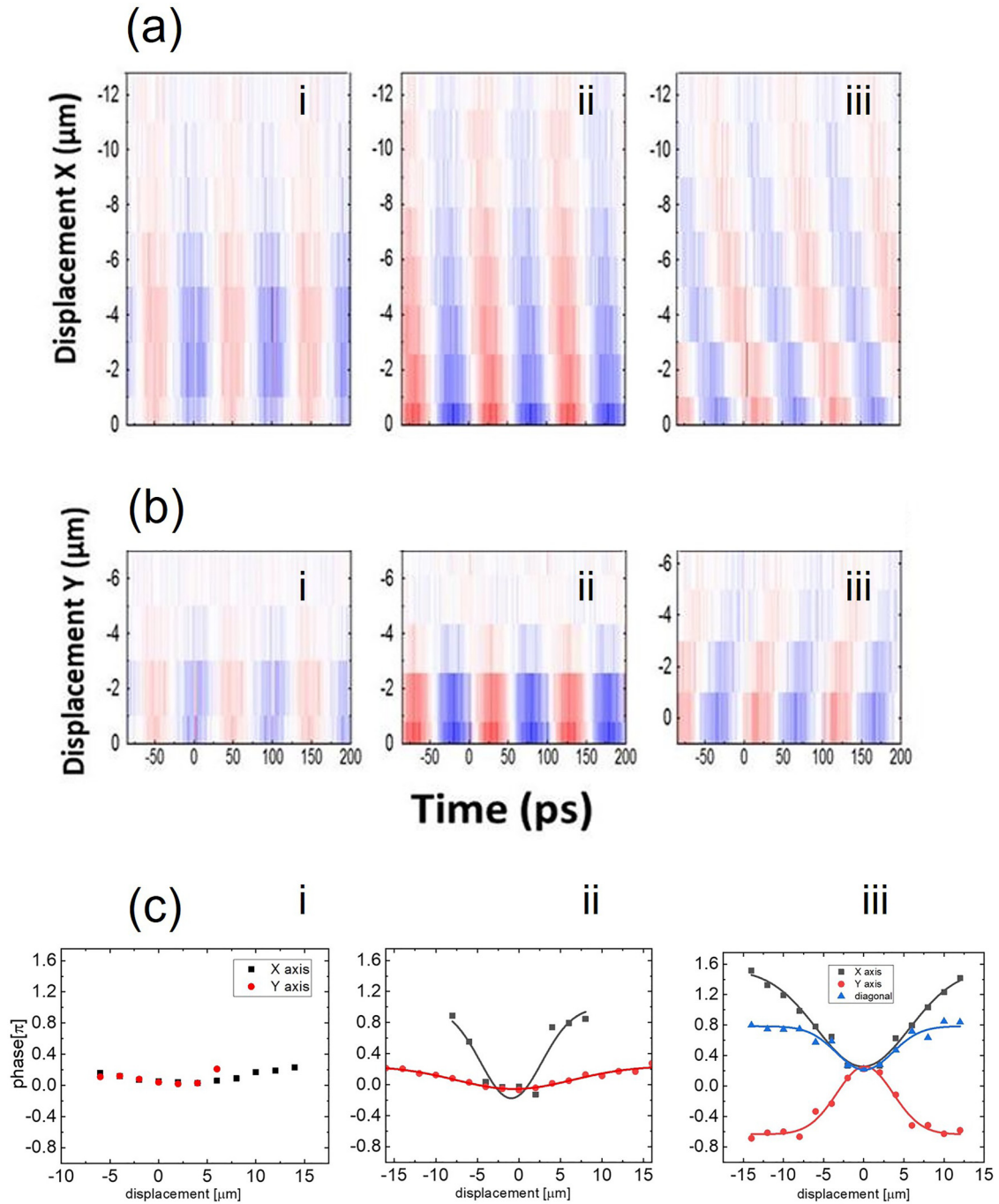


FIG. 3. Color maps of measured Faraday rotation angle showing the oscillations of the out-of-plane magnetization component in time and space. The scans are measured along the  $X$  axis (a) and  $Y$  axis (b). The panels in (c) give the phases of the probe signals for three different strengths of the external magnetic field. In each row three situations are shown: below the resonance,  $\Delta < 0$  ( $\Delta = -3.8 \times 10^{-2}$ )– $H = 3.33$  kOe [(a)i, (b)i, (c)i], at resonance,  $\Delta = 0$ – $H = 3.46$  kOe [(a)ii, (b)ii, (c)ii], and above the resonance,  $\Delta > 0$  ( $\Delta = 5.5 \times 10^{-2}$ )– $H = 3.66$  kOe [(a)iii, (b)iii, (c)iii]. Laser pulse repetition rate is 10 GHz.

The observed signals plotted for different distances between the pump and probe beams along the  $X$  and  $Y$  axes are shown in Figs. 3(a) and 3(b), which visualize the evolution of the precession phase  $\zeta(\xi)$ , where  $\xi$  is the displacement between the pump and probe beams [Fig. 3(c)], and readily give the average phase velocity of the MSW wave packet,  $v_{\text{ph}} = 2\pi \nu \left(\frac{\partial \zeta}{\partial \xi}\right)^{-1}$  for different detunings. For the shift along the  $X$  axis we find: below the resonance ( $\Delta = -3.75 \times 10^{-2}$ ),

at  $H = 3.33$  kOe,  $v_{\text{ph}} = -1.75 \times 10^3$  km/s, at the resonance ( $\Delta = 0$ ), at  $H = 3.48$  kOe,  $v_{\text{ph}} = -0.48 \times 10^3$  km/s, and above the resonance ( $\Delta = 5.53 \times 10^{-2}$ ), at  $H = 3.66$  kOe,  $v_{\text{ph}} = -0.18 \times 10^3$  km/s. Since  $\frac{\partial \zeta}{\partial \xi} < 0$  [see the red curves in Fig. 3(c)] the phase velocity is negative, which is due to the backward character of the MSW, and its modulus decreases with increasing  $\Delta$ , i.e., for larger magnetic fields. The MSW wavelength drops for increasing field from 175  $\mu\text{m}$  at  $H =$

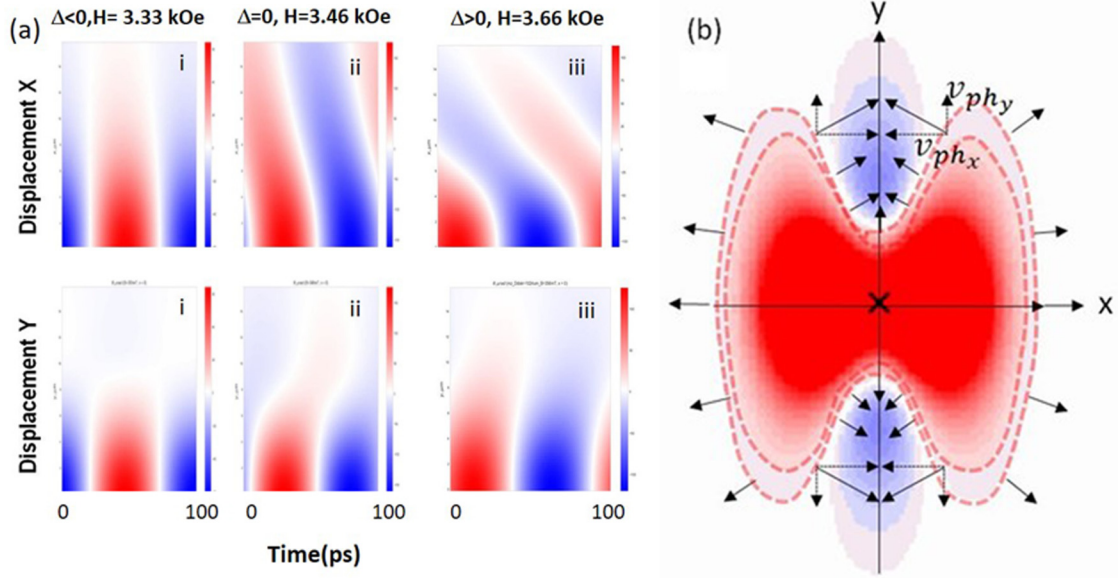


FIG. 4. (a) Color maps of the calculated spatial and temporal distribution of the amplitude of the out-of-plane magnetization component of the MSWs, represented by the amplitude of the Faraday rotation angle of the probe for three different values of the external magnetic field: (i) below the resonance  $\Delta = -3.8 \times 10^{-2} - H = 3.33$  kOe, (ii) at resonance  $\Delta = 0 - H = 3.46$  kOe, and (iii) above the resonance  $\Delta = 5.5 \times 10^{-2} - H = 3.66$  kOe. (b) Instant spatial distribution of the out-of-plane magnetization component of the MSWs at  $H = 3.66$  kOe. Isophases are shown with the dashed curves. Normals to the isophase curves give the direction of the phase velocity. Laser-pulse repetition rate is 10 GHz.

3.33 kOe to  $18 \mu\text{m}$  at  $H = 3.66$  kOe. The scans along the  $Y$  axis give a similar behavior but with a positive detuning  $\frac{\partial \zeta}{\partial \xi} > 0$  at  $\Delta > 0$ , so that the phase velocity gets positive [Fig. 3(c),iii] which turns out to be essential for the formation of the  $X$  shape at  $\Delta > 0$ , as will be discussed further in the theoretical section. Therefore, a small variation of the detuning  $\Delta$  under periodic pumping of a magnetic sample allows one to control the phase velocity and wavelength of the generated spin waves.

#### IV. THEORETICAL CALCULATIONS AND MICROMAGNETIC MODELING

In order to understand the mechanisms responsible for the observed directionality patterns, we perform an additional micromagnetic modeling which we consider as reliable.

Let us start from calculation of the signals spatially distributed along the  $X$  axis and  $Y$  axis [Fig. 4(a)]. They are in excellent agreement with the corresponding experimental signals in Figs. 3(a) and 3(b), and also confirm the negative (positive) phase velocity for the  $X$  displacement ( $Y$  displacement) at  $\Delta > 0$ . The sign of the phase velocity can be understood if one plots the instant distribution  $m_z(x, y)$  of the out-of-plane component of MSW for the resonant case [Fig. 4(b)]. The normal vectors to the isophase curves represent the direction of the phase velocity vector  $\mathbf{v}_{\text{ph}}$  at different points. Due to the peculiar dispersion of the MSW the isophases have rather complex shape and the distribution of  $\mathbf{v}_{\text{ph}}$  is anisotropic. Thus, at the points along the  $X$  axis,  $\mathbf{v}_{\text{ph}}$  is directed oppositely to the  $X$  axis, which explains the negative sign of  $v_{\text{ph}}$  observed in Figs. 3(a)i–iii and 4(a)i–iii.

In order to understand the spatial distribution of the magnetic oscillations for different magnetic fields (Figs. 3 and 4), let us consider the dispersion of the backward-volume MSWs, which is given by [29]

$$v(\mathbf{k}) = \frac{\gamma}{2\pi} \sqrt{H[H + H_a F(k_x, k_y)]}, \quad (5)$$

where  $F(k_x, k_y) = 1 + P(k)[1 - P(k)](\frac{H_a}{H})(\frac{k_y^2}{k^2}) - P(k)(\frac{k_x^2}{k^2})$ ,  $P(k) = 1 - \frac{1 - \exp(-kl)}{kl}$ , and  $k = \sqrt{k_x^2 + k_y^2}$ ,  $l$  is the film thickness. This dispersion relation is valid in the long-wavelength approximation  $kl < 1/2$ . The dispersion curves for MSWs propagating along the  $X$  axis in the sample for the three considered strengths of the magnetic field are shown in Fig. 5(a).

Focused pump pulses of radius  $r$  excite MSWs with momenta  $k < \frac{2}{r} = 0.5 \mu\text{m}^{-1}$  [15]. On the other hand, the efficiency of excitation of magnetization precession depends on its frequency and in accordance with Eq. (1) maximizes at  $\nu = 10$  GHz. In Fig. 5(a) the excitation efficiency is shown by gradient blue color, where a more intense color corresponds to a higher efficiency. At  $\Delta = -3.8 \times 10^{-2}$  all dispersion curves lie within the frequency range corresponding to relatively high excitation efficiency [the red curve in Fig. 5(a)]. However, for  $\Delta = 5.5 \times 10^{-2}$  only the long wave-vector part of dispersion falls into the range of excited frequencies [blue curve in Fig. 5(a)], while for  $\Delta = -3.8 \times 10^{-2}$  only near-zero wave vectors are attainable by the pulse train [the black curve in Fig. 5(a)]. This explains the highest spin-wave amplitude at  $\Delta = 0$ .

In order to understand the directionality patterns of the MSWs observed for three different external fields, let us consider the isofrequency curves  $k_y(k_x)$  corresponding to the

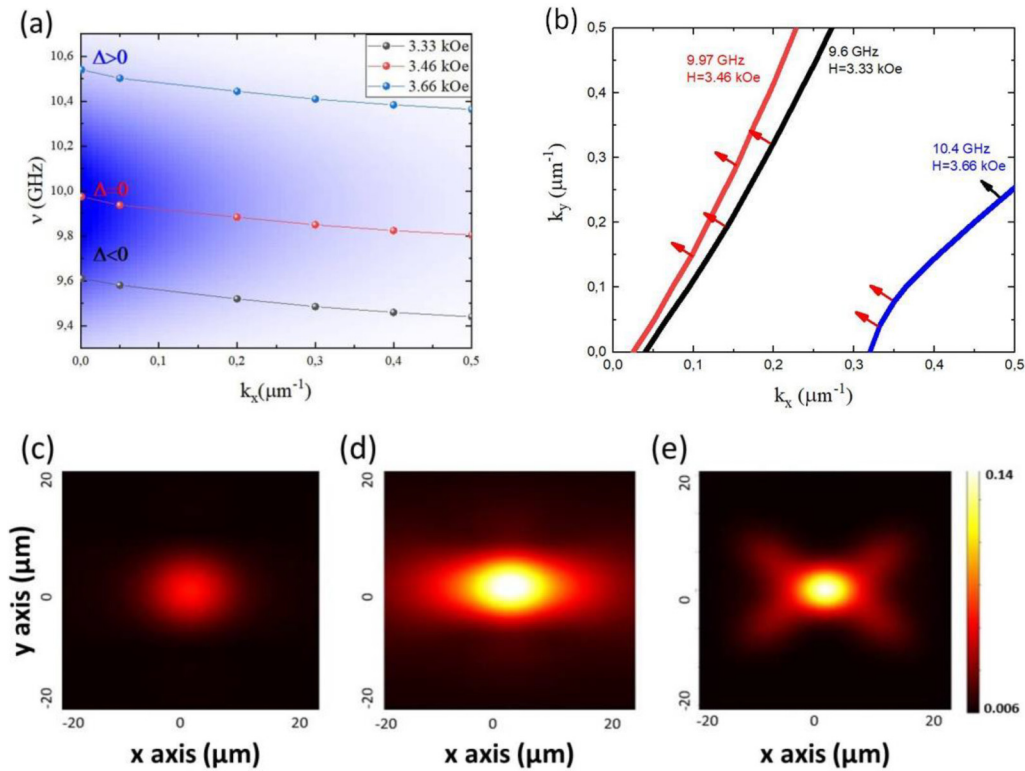


FIG. 5. (a), (b) Dispersion of backward MSW calculated according to Eq. (4) (a) and optimal isofrequency curves (b) for three external magnetic fields: 3.33 kOe ( $\Delta = -3.8 \times 10^{-2}$ ), 3.46 kOe ( $\Delta = 0$ ), and 3.66 kOe ( $\Delta = 5.5 \times 10^{-2}$ ). (c)–(e) Color maps of the calculated spatial distribution of the amplitude of the out-of-plane magnetization component of the MSWs at three different values of the external magnetic field: (c)  $H = 3.33$  kOe, (d)  $H = 3.46$  kOe, and (e)  $H = 3.66$  kOe.

frequencies optimal for MSW excitation at different detunings:  $\nu = 9.6$  GHz for  $\Delta < 0$  ( $H = 3.33$  kOe) [black curve in Fig. 5(b)],  $\nu = 10.0$  GHz for  $\Delta = 0$  [red curve in Fig. 5(b)], and  $\nu = 10.4$  GHz for  $\Delta > 0$  ( $H = 3.66$  kOe) [blue curve in Fig. 5(b)]. The group velocity of the MSW,  $\mathbf{v}_{gr}$ , is perpendicular to these curves (see red arrows). There is a notable difference between these three curves: while at  $\Delta < 0$  (black curve) and  $\Delta = 0$  (red curve) the second derivative of the isofrequency function  $k_y(k_x)$  keeps its sign at any accessible  $k_x$ , at  $\Delta > 0$  an inflection point appears at  $k_x = 0.48 \mu\text{m}^{-1}$ , which is favorable for the formation of a caustics [17]. The group velocity at this point is directed at around  $45^\circ$  relative to  $\mathbf{H}$  [black arrow in Fig. 5(b)]. As a result, the calculations give an X-shaped directionality pattern of the MSW [Fig. 5(e)], which is in good agreement with the experimental results [Fig. 2(c)]. The calculated MSW patterns at other magnetic fields are also in good agreement with the experimental distributions [Figs. 5(c) and 5(d) vs Figs. 2(a) and 2(b)].

## V. CONCLUSION

In conclusion, we compare the excitation of spin waves in an iron garnet film using high-frequency repetition-rate laser pulses at 1- and 10 GHz, matched to the ferromagnetic resonance. The use of high-frequency pumping allows one to selectively excite the spin waves of certain phase velocity

and wavelength, which can vary greatly under the action of small magnetic fields. Moreover, we show that for pulses with the same energy density, the extremely high repetition rate of 10 GHz leads to a more efficient resonant excitation of spin waves compared to a frequency of 1 GHz. In particular, it substantially narrows the spectrum of optically generated spin waves. This might be also crucial when there are limitations for the maximum energy per pulse that can be applied to a sample. Also, high-frequency pumping has the ability to change the directionality diagram of spin waves when the detuning between repetition rate and ferromagnetic resonance is varied, which can be accomplished by fine-tuning of the external magnetic field. The results obtained may be useful for controlling the frequency and directional spectrum of spin waves, which is important for magnonic devices.

## ACKNOWLEDGMENTS

This work was financially supported by a Russian Foundation of Basic Research (Project No. N 20-52-12047), and Deutsche Forschungsgemeinschaft (Project No. AK40/11-1). The growth of the iron garnet films was financially supported by the Russian Ministry of Education and Science, Megagrant Project No. N 075-15-2019-1934.



- [1] E. Beaurepaire, J.-C. Merle, A. Daunois, and J.-Y. Bigot, Ultrafast Spin Dynamics in Ferromagnetic Nickel, *Phys. Rev. Lett.* **76**, 4250 (1996).
- [2] C. D. Stanciu, A. V. Kimel, F. Hansteen, A. Tsukamoto, A. Itoh, A. Kirilyuk, and Th. Rasing, Ultrafast spin dynamics across compensation points in ferrimagnetic GdFeCo: The role of angular momentum compensation, *Phys. Rev. B* **73**, 220402(R) (2006).
- [3] M. Savoini, R. Medapalli, B. Koene, A. R. Khorsand, L. Le Guyader, L. Duo, M. Finazzi, A. Tsukamoto, A. Itoh, F. Nolting *et al.*, Highly efficient all-optical switching of magnetization in GdFeCo microstructures by interference-enhanced absorption of light, *Phys. Rev. B* **86**, 140404(R) (2012).
- [4] L. Le Guyader, M. Savoini, S. El Moussaoui, M. Buzzi, A. Tsukamoto, A. Itoh, A. Kirilyuk, T. Rasing, A. V. Kimel, and F. Nolting, Nanoscale sub-100 picosecond all-optical magnetization switching in GdFeCo microstructures, *Nat. Commun.* **6**, 1 (2015).
- [5] Y. Hashimoto, A. R. Khorsand, M. Savoini, B. Koene, D. Bossini, A. Tsukamoto, A. Itoh, Y. Ohtsuka, K. Aoshima, A. V. Kimel, and others, Ultrafast time-resolved magneto-optical imaging of all-optical switching in GdFeCo with femtosecond time-resolution and a  $\mu\text{m}$  spatial-resolution, *Rev. Sci. Instrum.* **85**, 63702 (2014).
- [6] A. V. Kimel, A. Kirilyuk, P. A. Usachev, R. V. Pisarev, A. M. Balbashov, and T. Rasing, Ultrafast non-thermal control of magnetization by instantaneous photomagnetic pulses, *Nature (London)* **435**, 655 (2005).
- [7] F. Hansteen, A. Kimel, A. Kirilyuk, and T. Rasing, Nonthermal ultrafast optical control of the magnetization in garnet films, *Phys. Rev. B* **73**, 014421 (2006).
- [8] A. I. Chernov, M. A. Kozhaev, I. V. Savochkin, D. V. Dodonov, P. M. Vetoshko, A. K. Zvezdin, and V. I. Belotelov, Optical excitation of spin waves in epitaxial iron garnet films: MSSW vs BVMSW, *Opt. Lett.* **42**, 279 (2017).
- [9] A. I. Chernov, M. A. Kozhaev, A. Khranova, A. N. Shaposhnikov, A. R. Prokopov, V. N. Berzhansky, A. K. Zvezdin, and V. I. Belotelov, Control of the phase of the magnetization precession excited by circularly polarized femtosecond-laser pulses, *Photonics Res.* **6**, 1079 (2018).
- [10] M. Jäckl, V. I. Belotelov, I. A. Akimov, I. V. Savochkin, D. R. Yakovlev, A. K. Zvezdin, and M. Bayer, Magnon Accumulation by Clocked Laser Excitation as Source of Long-Range Spin Waves in Transparent Magnetic Films, *Phys. Rev. X* **7**, 021009 (2017).
- [11] C.-H. Lambert, S. Mangin, B. S. D. Ch. S. Varaprasad, Y. K. Takahashi, M. Hehn, M. Cinchetti, G. Malinowski, K. Hono, Y. Fainman, M. Aeschlimann *et al.*, All-optical control of ferromagnetic thin films and nanostructures, *Science* **345**, 1337 (2014).
- [12] F. Atoneche, A. M. Kalashnikova, A. V. Kimel, A. Stupakiewicz, A. Maziewski, A. Kirilyuk, and Th. Rasing, Large ultrafast photoinduced magnetic anisotropy in a cobalt-substituted yttrium iron garnet, *Phys. Rev. B* **81**, 214440 (2010).
- [13] T. Satoh, Y. Terui, R. Moriya, B. A. Ivanov, K. Ando, E. Saitoh, T. Shimura, and K. Kuroda, Directional control of spin-wave emission by spatially shaped light, *Nat. Photonics* **6**, 662 (2012).
- [14] K. Matsumoto, I. Yoshimine, K. Himeno, T. Shimura, and T. Satoh, Observation of evanescent spin waves in the magnetic dipole regime, *Phys. Rev. B* **101**, 184407 (2020).
- [15] D. M. Krichevsky, D. O. Ignatyeva, V. A. Ozerov, and V. I. Belotelov, Selective and Tunable Excitation of Standing Spin Waves in a Magnetic Dielectric Film by Optical Guided Modes, *Phys. Rev. Appl.* **15**, 034085 (2021).
- [16] L. P. Pitaevskii, Electric forces in a transparent dispersive medium, *Sov. Phys. JETP* **12**, 1008 (1961).
- [17] P. S. Pershan, Nonlinear optical properties of solids: Energy considerations, *Phys. Rev.* **130**, 919 (1963).
- [18] M. A. Kozhaev, A. I. Chernov, D. A. Sylgacheva, A. N. Shaposhnikov, A. R. Prokopov, V. N. Berzhansky, A. K. Zvezdin, and V. I. Belotelov, Giant peak of the inverse Faraday effect in the band gap of magnetophotonic microcavity, *Sci. Rep.* **8**, 1 (2018).
- [19] I. V. Savochkin, M. Jäckl, V. I. Belotelov, I. A. Akimov, M. A. Kozhaev, D. A. Sylgacheva, A. I. Chernov, A. N. Shaposhnikov, A. R. Prokopov, V.N. Berzhansky, and others, Generation of spin waves by a train of fs-laser pulses: A novel approach for tuning magnon wavelength, *Sci. Rep.* **7**, 1 (2017).
- [20] A. A. Awad, S. Muralidhar, A. Alemán, R. Khymyn, D. Hanstorp, and J. Åkerman, Femtosecond laser comb driven perpendicular standing spin waves, *Appl. Phys. Lett.* **120**, 12405 (2022).
- [21] A. Aleman, S. Muralidhar, A. A. Awad, J. Åkerman, and D. Hanstorp, Frequency comb enhanced Brillouin microscopy, *Opt. Express* **28**, 29540 (2020).
- [22] S. Muralidhar, A. A. Awad, A. Alemán, R. Khymyn, M. Dvornik, D. Hanstorp, and J. Åkerman, Sustained coherent spin wave emission using frequency combs, *Phys. Rev. B* **101**, 224423 (2020).
- [23] S. Muralidhar, R. Khymyn, A. A. Awad, A. Alemán, D. Hanstorp, and J. Åkerman, Femtosecond Laser Pulse Driven Caustic Spin Wave Beams, *Phys. Rev. Lett.* **126**, 037204 (2021).
- [24] M. Kobecki, A. V. Scherbakov, T. L. Linnik, S. M. Kukhtaruk, V. E. Gusev, D. P. Pattnaik, I. A. Akimov, A. W. Rushforth, A. V. Akimov, and M. Bayer, Resonant thermal energy transfer to magnons in a ferromagnetic nanolayer, *Nat. Commun.* **11**, 1 (2020).
- [25] O. Madelung, *Landolt-Bornstein Group III: Condensed Matter* (Springer-Verlag, 1983).
- [26] A. Kirilyuk, A. V. Kimel, and T. Rasing, Ultrafast optical manipulation of magnetic order, *Rev. Mod. Phys.* **82**, 2731 (2010).
- [27] A. E. Khranova, M. Kobecki, I. A. Akimov, I. V. Savochkin, M. A. Kozhaev, A. N. Shaposhnikov, V. N. Berzhansky, A. K. Zvezdin, M. Bayer, and V. I. Belotelov, Accumulation and control of spin waves in magnonic dielectric microresonators by a comb of ultrashort laser pulses, *Sci. Rep.* **12**, 7369 (2022).
- [28] K. Ali, M. Z. Akbar, M. F. Iqbal, and M. Ashraf, Numerical simulation of heat and mass transfer in unsteady nanofluid between two orthogonally moving porous coaxial disks, *AIP Adv.* **4**, 107113 (2014).
- [29] J. Miltat, G. Albuquerque, D. Burkard Hillebrands, and K. Ounadjela, Spin dynamics in confined magnetic structures I, (2002).